

Beam dynamics framework incorporating acceleration to define the minimum aperture in two focusing schemes for proton radiotherapy linac

M. Southerby^{*} and R. Apsimon[†]

*Engineering Department, Lancaster University, Lancaster LA1 4YW, United Kingdom
and Cockcroft Institute, Daresbury Laboratory, Warrington WA4 4AD, United Kingdom*



(Received 20 March 2024; accepted 21 May 2024; published 4 June 2024)

In this paper, a self-consistent transverse beam dynamics framework is demonstrated that incorporates acceleration into the transverse beam dynamics studies for a proton linac machine. Two focusing schemes are developed and discussed: the FODO-like scheme and the minimum aperture scheme. The FODO-like scheme is a simple scheme, requiring only one quadrupole per cavity. The scheme is analytically solved to minimize the beam size at the cavity entrance/exit and ensures a constant beam size along the lattice, with respect to adiabatic damping due to longitudinally accelerating rf cavities. The minimum aperture scheme describes the regime that matches the beam ellipse to the acceptance ellipse of a cavity, allowing for the smallest possible aperture, for a given cavity length. A simple approximation of an rf cavity map is determined to allow changes in particle energy along a lattice, and acceleration is assumed only in the longitudinal direction.

DOI: [10.1103/PhysRevAccelBeams.27.064401](https://doi.org/10.1103/PhysRevAccelBeams.27.064401)

I. INTRODUCTION

In the recent decades, all-linac solutions for proton acceleration with medical applications have become an increasing area of interest [1]. Two areas to have benefited from such improvements are cancer radiotherapy and medical imaging [2,3]. All-linac solutions have benefits over the conventional cyc-linac and synchrotron machines with respect to energy and intensity modulated on the scale of ms. This allows for more efficient treatment of cancers with proton beams, such as active spot scanning for moving organs [4]. In addition to advantages to radiotherapy, linac boosters can be used in conjunction with cyc-linac or all-linac solutions to push proton energy to 350 MeV, the energy required for medical imaging [5]. Proton medical imaging allows a more accurate calculation of the required proton energy during radiotherapy, over conventional x-ray imaging, due to the proton stopping power.

All-linac machines benefit from a smaller beam emittance than cyc-linac machines, and therefore, can operate with smaller beam apertures, increasing the shunt impedance. Limits are often placed on the beam aperture due to

the transverse focusing requirements of the linac, in addition to peak fields and power coupling.

This paper describes the method used to minimize the beam aperture with respect to transverse beam losses, for a given cavity length, analytically. This paper will discuss two focusing schemes: namely the FODO-like scheme and the minimum aperture scheme (MAS), incorporating longitudinal momentum gain. The FODO-like scheme is similar to the well-known FODO scheme, comprised of quadrupole of alternating polarity to produce a net focusing force transversely. The MAS scheme produces a matching section that aligns the transverse beam ellipse with the cavity acceptance ellipse. An rf cavity transfer map is produced to simulate longitudinal acceleration of protons, and the corresponding adiabatic damping that occurs as a result. Due to the very low beam currents used in proton radiotherapy linacs [6] (of the order nA), space-charge effects are ignored.

The Twiss parameter transfer matrix is adapted to account for the change in beam emittance due to acceleration. The method requires minimizing the Twiss beta function, β , at the cavity entrance and exit to minimize the beam aperture for a given cavity length and beam emittance, while ensuring maximum beam acceptance.

II. TWISS PARAMETERS WITH ACCELERATION

The phase space ellipse of a particle in a periodic beam line, with geometric emittance $\epsilon_{g,x}$, is described

$$\epsilon_{g,x} = \beta_x x'^2 + 2\alpha_x x x' + \gamma_x x^2, \quad (1)$$

^{*}m.southerby@lancaster.ac.uk

[†]r.apsimon@lancaster.ac.uk

Published by the American Physical Society under the terms of the Creative Commons Attribution 4.0 International license. Further distribution of this work must maintain attribution to the author(s) and the published article's title, journal citation, and DOI.

where β_x , α_x , and $\gamma_x = \frac{1+\alpha_x^2}{\beta_x}$ are the Twiss parameters in x [7], x is the transverse size of the beam, and $x' = \frac{dx}{ds} = \frac{p_x}{p_z}$ for longitudinal displacement, s . The maximum beam size at any point s is given $\sigma = x_{\max} = \sqrt{\beta(s)\varepsilon_g(s)}$.

It is required to use the Lorentz invariant normalized emittance, defined as $\varepsilon_n = \varepsilon_g(s)\gamma_r(s)\beta_r(s)$ [7], where $\gamma_r(s)$, $\beta_r(s)$ are the Lorentz factor and normalized particle velocity, respectively. Using Eq. (1) to equate the normalized emittance of a particle before and after an rf cavity:

$$\begin{aligned} & \gamma_{r0}\beta_{r0}(\beta_{x1}x_1'^2 + 2\alpha_{x1}x_1x_1' + \gamma_{x1}x_1^2) \\ &= \gamma_{r1}\beta_{r1}(\beta_{x0}x_0'^2 + 2\alpha_{x0}x_0x_0' + \gamma_{x0}x_0^2), \end{aligned} \quad (2)$$

where $\gamma_{r0}\beta_{r0}$ and $\gamma_{r1}\beta_{r1}$ are the Lorentz factor and normalized particle velocity at the start and end of the cavity, respectively. The cavity can be described with a linear transfer map, R :

$$\begin{pmatrix} x_1 \\ x_1' \end{pmatrix} = \begin{pmatrix} R_{11} & R_{12} \\ R_{21} & R_{22} \end{pmatrix} \begin{pmatrix} x_0 \\ x_0' \end{pmatrix}. \quad (3)$$

Assuming only longitudinal acceleration, the divergence before and after the cavity is given

$$x_1' = \frac{\Delta p_x + x_0' p_{z0}}{p_{z1}}, \quad (4)$$

where Δp_x can be determined from Lorentz force, for a particle of charge q , longitudinal velocity $\beta_z c$, and at azimuthal angle θ :

$$\Delta p_x = q \cos(\theta) \left(\frac{\int E_r dz}{\beta_{rz} c} + \int B_\theta dz \right). \quad (5)$$

In an azimuthally symmetric cylindrical cell, the radial electric field (E_r) and azimuthal magnetic field (B_θ) can be written as functions of the longitudinal electric field, E_z , using a first order expansion about $r = 0$:

$$E_r = -\frac{r}{2} \frac{dE_z}{dz}, \quad B_\theta = \frac{\omega r}{2c^2} E_z, \quad (6)$$

where ω is the angular frequency. A typical E_z field component can be written as a Fourier series [8], with the most simple case being:

$$E_z = \sin\left(\frac{\pi z}{L_{\text{cell}}}\right) \sin(\omega t + \phi_0), \quad (7)$$

for a given cell length, L_{cell} . ϕ_0 represents the mean phase over the cavity. The value of E_z as observed by a particle at constant velocity can be determined by substituting $t = \frac{z}{\beta_z c}$ into Eq. (7).

Using Eqs. (7), (6), (5), and (4) produces an approximation for x_1' :

$$x_1' = \frac{N\pi}{4p_{z1}} \left(\beta_{rz0} - \frac{1}{\beta_{rz0}} \right) \sin(\phi_0) x_0 + \frac{p_{z0}}{p_{z1}} x_0, \quad (8)$$

where N is the number of rf cells in the rf cavity, and $NL_{\text{cell}} = L_{\text{cav}}$. Integrating Eq. (8) over the cavity length produces a similar form for x_1 . The final result of the cavity map is shown below:

$$\mathbf{R} = \begin{pmatrix} 1 + \frac{N\pi}{4} \left(\beta_{rz0} - \frac{1}{\beta_{rz0}} \right) \sin(\phi_0) L' & \gamma_{r0} \beta_{rz0} m c L' \\ \frac{N\pi}{4\gamma_{rs} \beta_{rz1} m c} \left(\beta_{rz0} - \frac{1}{\beta_{rz0}} \right) \sin(\phi_0) & A_d \end{pmatrix}, \quad (9)$$

where

$$\begin{aligned} L' &= \frac{L_{\text{cav}}}{\Delta\gamma \cos(\phi_0) m c} (\cosh^{-1}[\gamma_{r0} + \Delta\gamma \cos(\phi_0)] \\ &\quad - \cosh^{-1}(\gamma_{r0})), \end{aligned} \quad (10)$$

with $\Delta\gamma = \gamma_{r1} - \gamma_{r0}$, and

$$A_d = \left(1 + \Delta\gamma \cos(\phi_0) \frac{\Delta\gamma \cos(\phi_0) + 2\gamma_{r0}}{\gamma_{r0}^2 - 1} \right)^{-1/2}. \quad (11)$$

To proceed, the rf phase is chosen such that longitudinal acceleration is maximized, and defocusing forces are minimized, $\phi_0 = 0$, as these are the conditions of the ideal particle:

$$\mathbf{R} = \begin{pmatrix} 1 & L_{\text{cav}} \frac{\gamma_{r0}\beta_{rz0}}{\gamma_{r1}-\gamma_{r0}} \ln\left(\frac{\gamma_{r1}\beta_{rz1}+\gamma_{r1}}{\gamma_{r0}\beta_{rz0}+\gamma_{r0}}\right) \\ 0 & \frac{\gamma_{r0}\beta_{rz0}}{\gamma_{r1}\beta_{rz1}} \end{pmatrix}. \quad (12)$$

The transfer matrices described in Eqs. (9) and (12) are related to the well-known transfer matrix derived by Rosenzweig and Serafini [9]. However, the Rosenzweig-Serafini (RS) matrix assumes ultrarelativistic particles, whereas the derivation described in this article is extended to partially relativistic particles, which is more appropriate when modeling protons. In addition, the RS formalism averages the periodic radial force experienced by charged particles in an rf cavity. Furthermore, the RS matrix includes focusing and defocusing terms from the fringe fields at the start and end of the cavity, although this could be easily incorporated into Eqs. (9) and (12) if required, by including the same edge-focusing terms that Rosenzweig and Serafini use. The Twiss parameter transfer matrix can be derived by substituting x_0, x_0' as functions of x_1, x_1' [using the inverse form for Eq. (3)] into Eq. (2):

$$\begin{pmatrix} \beta_{x1} \\ \alpha_{x1} \\ \gamma_{x1} \end{pmatrix} = \frac{\gamma_{r1}\beta_{r1}}{\gamma_{r0}\beta_{r0}} \begin{pmatrix} R_{11}^2 & -2R_{11}R_{12} & R_{12}^2 \\ -R_{11}R_{21} & R_{11}R_{22} + R_{12}R_{21} & -R_{12}R_{22} \\ R_{21}^2 & -2R_{21}R_{22} & R_{22}^2 \end{pmatrix} \times \begin{pmatrix} \beta_{x0} \\ \alpha_{x0} \\ \gamma_{x0} \end{pmatrix}. \quad (13)$$

The Twiss parameter transfer matrix takes on the recognized form for zero acceleration, when $\frac{\gamma_{r1}\beta_{r1}}{\gamma_{r0}\beta_{r0}} = 1$, as expected.

The basic start point has now been established, with a simple cavity transfer map, and the Twiss parameter transfer matrix incorporating acceleration.

III. FODO-LIKE SCHEME

The aim of the FODO-like scheme is to analytically provide the quadrupole k -strength and length such that the beam size is minimized at the cavity entrance/exit, producing the smallest beam aperture possible for a given chosen cavity length.

The lattice starts at a location such that the Twiss alpha function is 0 in both transverse planes:

$$\alpha_{x0} = \alpha_{y0} = 0. \quad (14)$$

It is arbitrarily chosen:

$$\beta_x = \text{Max}, \quad \beta_y = \text{Min}. \quad (15)$$

The focusing scheme is a periodic array of the following elements, constructing the FODO cell:

$$[\text{half-FQ}][\text{drift}][\text{DQ}][\text{drift}][\text{half-FQ}]. \quad (16)$$

It is convenient to split the FODO cell into half-FODO cells, where the split is at some point within the DQ such that $\alpha_{x1} = \alpha_{y1} = 0$. For zero acceleration, the split is at the

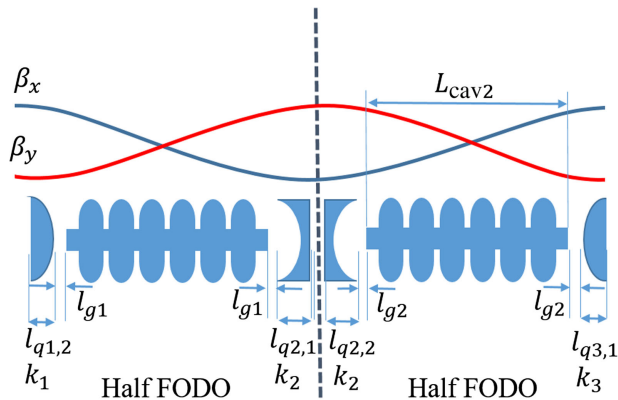


FIG. 1. FODO-like schematic.

midpoint. The drift sections are replaced with cavity sections, sandwiched between short drift lengths, of length l_g , to closer approximate a realistic beam line. The half focusing quadrupoles are described with length $l_{q1,2}$ [where the second index (2) refers to the quadrupole being the second half of a complete quadrupole] and strength k_1 , where $k = \frac{1}{B\rho} \frac{\partial B_y}{\partial x}$ and $B\rho$ is the magnetic rigidity, as shown in Fig. 1. For now, the second quadrupole index is dropped ($l_{q1,2} = l_{q1}$).

The half-FODO cell in the x plane is thus:

$$\mathbf{M} = [\text{half-FQ}][\text{drift}][\text{cavity}][\text{drift}][\text{half-DQ}]. \quad (17)$$

Explicitly, the transfer map is as follows:

$$\mathbf{M} = \begin{pmatrix} \cosh(\sqrt{k_2}l_{q2}) & \frac{1}{\sqrt{k_2}}\sinh(\sqrt{k_2}l_{q2}) \\ \sqrt{k_2}\sinh(\sqrt{k_2}l_{q2}) & \cosh(\sqrt{k_2}l_{q2}) \end{pmatrix} \times \begin{pmatrix} 1 & L_{\text{eff}} \\ 0 & \frac{\gamma_{r0}\beta_{r0}}{\gamma_{r1}\beta_{r1}} \end{pmatrix} \begin{pmatrix} \cos(\sqrt{k_1}l_{q1}) & \frac{1}{\sqrt{k_1}}\sin(\sqrt{k_1}l_{q1}) \\ -\sqrt{k_1}\sin(\sqrt{k_1}l_{q1}) & \cos(\sqrt{k_1}l_{q1}) \end{pmatrix}. \quad (18)$$

Where the [drift][cavity][drift] matrix has been multiplied together, and

$$L_{\text{eff}} = l_g \left(\frac{\gamma_{r0}\beta_{r0}}{\gamma_{r1}\beta_{r1}} + 1 \right) + l_{\text{cav}} \frac{\gamma_{r0}\beta_{r0}}{\gamma_{r1} - \gamma_{r0}} \ln \left(\frac{\gamma_{r1}\beta_{r1} + \gamma_{r1}}{\gamma_{r0}\beta_{r0} + \gamma_{r0}} \right). \quad (19)$$

Using Eq. (13) to transform the Twiss parameters due to transfer map M from $\alpha_{x0} = 0$ to $\alpha_{x1} = 0$:

$$0 = -M_{11}M_{21}\beta_{x0} - \frac{M_{12}M_{22}}{\beta_{x0}}. \quad (20)$$

This produces an analytical form for the Twiss β functions at the start of the half-FODO cell, as functions of the half-FODO transfer map M :

$$\beta_{x0} = \sqrt{\frac{-M_{12}M_{22}}{M_{11}M_{21}}}, \quad \beta_{y0} = \sqrt{\frac{-M_{34}M_{44}}{M_{33}M_{43}}}. \quad (21)$$

Enforcing the beam size in x at the start of the half-FODO is equal to the y beam size at the end of the half-FODO:

$$\sigma_{x0} = \sigma_{y1}, \quad \sigma_{x1} = \sigma_{y0}. \quad (22)$$

The beam size can be determined with the following:

$$\sigma = \sqrt{\frac{\beta \epsilon_n}{\gamma_r \beta_r}}, \quad (23)$$

therefore, Eq. (22) becomes

$$\frac{\gamma_{r1} \beta_{r1}}{\gamma_{r0} \beta_{r0}} \beta_{x0} = \beta_{y1}, \quad \frac{\gamma_{r1} \beta_{r1}}{\gamma_{r0} \beta_{r0}} \beta_{y0} = \beta_{x1}. \quad (24)$$

Therefore,

$$\beta_{x0} \beta_{x1} = \beta_{y0} \beta_{y1}. \quad (25)$$

The ratio of the β functions at each half-FODO cell, r , is given

$$\frac{\beta_{x0}}{\beta_{y0}} = \frac{\beta_{y1}}{\beta_{x1}} = r. \quad (26)$$

The Twiss β and γ functions at the end of the half-FODO can be determined using Eq. (13):

$$\beta_{x1} = \frac{\gamma_{r1} \beta_{r1}}{\gamma_{r0} \beta_{r0}} \left(M_{11}^2 \beta_{x0} + \frac{M_{12}^2}{\beta_{x0}} \right), \quad (27)$$

$$\beta_{y1} = \frac{\gamma_{r1} \beta_{r1}}{\gamma_{r0} \beta_{r0}} \left(M_{33}^2 \beta_{y0} + \frac{M_{34}^2}{\beta_{y0}} \right), \quad (28)$$

$$\gamma_{x1} = \frac{1}{\beta_{x1}} = \frac{\gamma_{r1} \beta_{r1}}{\gamma_{r0} \beta_{r0}} \left(M_{21}^2 \beta_{x0} + \frac{M_{22}^2}{\beta_{x0}} \right), \quad (29)$$

$$\gamma_{y1} = \frac{1}{\beta_{y1}} = \frac{\gamma_{r1} \beta_{r1}}{\gamma_{r0} \beta_{r0}} \left(M_{43}^2 \beta_{y0} + \frac{M_{44}^2}{\beta_{y0}} \right). \quad (30)$$

Combining the above equations, along with Eqs. (21), (25), and the equality $\det(M_x) = \det(M_y)$, it can be shown

$$M_{12} = \pm M_{34}, \quad M_{21} = \pm M_{43}$$

and

$$M_{11} M_{22} = M_{33} M_{44}. \quad (31)$$

Now that the basic relationships between half-FODO cell elements have been determined, it is required to expand the elements as functions of quadrupole, drift length, and cavity parameters. In order to proceed, quadrupole maps are simplified using the semithin lens approximation.

The semithin lens approximation expands trigonometric and hyperbolic functions and truncates at second order. For sensible values of k_1 and l_{q1} ; $k_1 l_{q1} \sim 1$, $k_1 l_{q1}^2 < 1$, and $k_1 l_{q1}^3 \ll 1$. Therefore, terms of the order $k_1^n l_{q1}^{n+2}$ are ignored in the semithin lens approximation, for any integer n :

$$\cos(\sqrt{k_1} l_{q1}) \approx 1 - k_1 l_{q1}^2 / 2,$$

$$\sin(\sqrt{k_1} l_{q1}) \approx \sqrt{k_1} l_{q1},$$

$$\cosh(\sqrt{k_1} l_{q1}) \approx 1 + k_1 l_{q1}^2 / 2,$$

$$\sinh(\sqrt{k_1} l_{q1}) \approx \sqrt{k_1} l_{q1}.$$

It also assumed that $l_g \sim l_{q1}$, thus any terms of the order $k_1^n l_g^{n+2}$ are also ignored.

Substituting the semithin lens approximations into Eq. (18), it is possible to show that the results in Eq. (31) can be simplified to the following identities:

$$k_1 l_{q1}^2 = k_2 l_{q2}^2, \quad (32)$$

$$l_{q1} = \frac{\gamma_{r0} \beta_{r0}}{\gamma_{r1} \beta_{r1}} l_{q2}, \quad (33)$$

$$k_1 = \frac{\gamma_{r1} \beta_{r1}^2}{\gamma_{r0} \beta_{r0}^2} k_2, \quad (34)$$

$$\frac{\gamma_{r0} \beta_{r0}}{\gamma_{r1} \beta_{r1}} k_1 l_{q1} = k_2 l_{q2}. \quad (35)$$

For zero acceleration, Eqs. (33)–(35) return to the expected case. The above results are also solutions for full order quadrupole elements.

In order to find the minimum aperture possible for a given cavity length, the β_x / β_y function at the start/end of the cavity is at a minimum. The transfer map, Λ_x , that transforms phase space from the initial position to the cavity entrance in x is a (semithin lens) focusing quadrupole of length l_{q1} followed by a drift of length l_g :

$$\Lambda = \begin{pmatrix} 1 & l_g \\ 0 & 1 \end{pmatrix} \begin{pmatrix} 1 - k_1 l_{q1}^2 / 2 & l_{q1} \\ -k_1 l_{q1} & 1 - k_1 l_{q1}^2 / 2 \end{pmatrix}. \quad (36)$$

The β function at the cavity entrance, β_{xc0} , is determined using Eqs. (13) and (36):

$$\beta_{xc0} = \Lambda_{11}^2 \beta_{x0} + \frac{\Lambda_{12}^2}{\beta_{x0}}. \quad (37)$$

β_{xc0} is minimized by differentiating Eq. (37) with respect to quadrupole parameters, k_1 , and equating to 0. It was found that differentiating with respect to l_{q1} was not optimal, as produces quadrupole lengths of the order 1 m:

$$\frac{d\beta_{xc0}}{dk_1} = 2\Lambda_{11} \frac{d\Lambda_{11}}{dk_1} \beta_{x0} + \Lambda_{11}^2 \frac{d\beta_{x0}}{dk_1} + 2\Lambda_{12} \frac{d\Lambda_{12}}{dk_1} \frac{1}{\beta_{x0}} - \Lambda_{12}^2 \frac{1}{\beta_{x0}^2} \frac{d\beta_{x0}}{dk_1} = 0. \quad (38)$$

Rearranging for the derivative of β_{x0} with respect to k_1 :

$$\frac{d\beta_{x0}}{dk_1} = \frac{-2\Lambda_{11}\beta_{x0}\frac{d\Lambda_{11}}{dk_1} - 2\Lambda_{12}\beta_{x0}^{-1}\frac{d\Lambda_{12}}{dk_1}}{\Lambda_{11}^2 - \Lambda_{12}^2\beta_{x0}^{-2}}. \quad (39)$$

A form for β_{x0} can be computed in the semithin lens regime using Eq. (21). The result is

$$\beta_{x0} \approx \frac{\sqrt{r}}{k_1 l_{q1}} \sqrt{1 + \frac{l_{q1}}{L_{\text{eff},1}}}, \quad (40)$$

which is subsequently differentiated with respect to k_1

$$\frac{d\beta_{x0}}{dk_1} = \beta_{x0} \left(\frac{1}{2r} \frac{dr}{dk_1} - \frac{1}{k_1} \right). \quad (41)$$

The aspect ratio, r , can be expanded in the semithin lens regime:

$$r = \frac{M_{33}}{M_{11}} \approx \frac{1 + L_{\text{eff},1} k_1 l_{q1} + k_1 l_{q1}^2 - \frac{L_{\text{eff},1} k_1^2 l_{q1}^3}{2}}{1 - L_{\text{eff},1} k_1 l_{q1} - k_1 l_{q1}^2 - \frac{L_{\text{eff},1} k_1^2 l_{q1}^3}{2}}, \quad (42)$$

which can be differentiated with respect to k_1 , as required in Eq. (41). Combining Eqs. (36), (39)–(42), before simplifying and ignoring all terms smaller than the semithin lens limit, produces a cubic in k_1 :

$$\begin{aligned} & -\frac{l_{q1}^4 L_{\text{eff}}^2}{2} k_1^3 + l_{q1}^2 (2l_g L_{\text{eff}} - 2l_{q1} L_{\text{eff}} - L_{\text{eff}}^2) k_1^2 \\ & - l_{q1} (L_{\text{eff}} + l_{q1}) k_1 + 1 = 0. \end{aligned} \quad (43)$$

It can be shown that for reasonable values for $l_{q1}, k_1, L_{\text{eff}}$, Eq. (43) has three real roots, and thus trigonometric solutions exist [10]. The solutions are as follows for $m = 0, 1, 2$:

$$k_1 = 2\sqrt{\frac{-p}{3}} \cos \left(\arccos \left(\frac{3q}{2p} \right) \sqrt{\frac{-1}{3p} - \frac{2\pi m}{3}} \right) - \frac{b}{3a}, \quad (44)$$

where

$$p = \frac{3ac - b^2}{3a^2}, \quad q = \frac{2b^3 - 9abc + 27a^2}{27a^3},$$

and

$$\begin{aligned} a &= \frac{-L_{\text{eff},1}^2 l_{q1}^4}{2}, \\ b &= l_{q1}^2 L_{\text{eff},1} (2(l_g - l_{q1}) - L_{\text{eff},1}), \\ c &= -l_{q1} (L_{\text{eff},1} + l_{q1}). \end{aligned}$$

Equation (43) can also be solved using the thin lens approximation, keeping terms of the form $k_1^n l_{q1}^m$. The result is

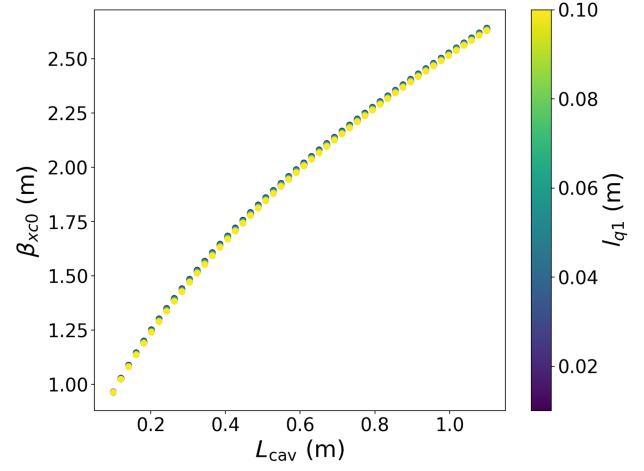


FIG. 2. Optimum value of β_{xc0} as a function of cavity length and the first quadrupole length.

$$k_1 = \frac{1}{l_{q1} L_{\text{eff},1}} \frac{\sqrt{5} - 1}{2}. \quad (45)$$

Equations (44) and (45) produce analytical methods to determine the optimum value of k_1 such that the maximum transverse beam size is minimized at the cavity entrance/exit, for a given cavity length and quadrupole length, within a FODO-like scheme.

It can be shown that the value of β_{xc0} is relatively insensitive to l_{q1} . As a result, the user defined value of l_{q1} is not heavily constrained. However, as the semithin lens regime is adopted, l_{q1} cannot approach similar values to l_{cav} . Figure 2 displays β_{xc0} as a function of cavity length and l_{q1} . The value of k_1 is calculated with Eq. (44). For

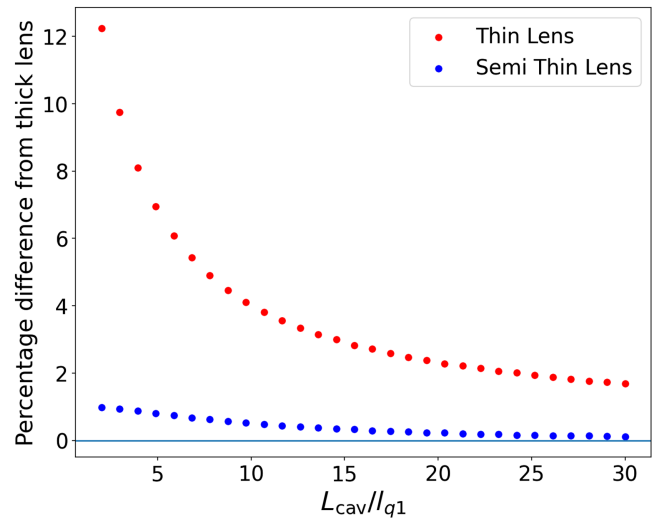


FIG. 3. Percentage difference between optimal value of k_1 as calculated by thick lens and the thin and semithin regimes. $l_{q1} = 0.05$ m, $l_g = 0.05$ m.

longer cavity lengths, β_{xc0} is larger, as expected. The value of β_{xc0} is highly insensitive to initial values of l_{q1} .

A. Semithin lens relative to thin lens

Figure 3 displays the percentage difference between the optimal value of k_1 as calculated by the thick lens regime (solved numerically) and the thin/semithin regimes. For the minimum ratio $L_{\text{cav}}/l_{q1} = 2$, the percentage difference between the semithin and thick lens regime is less than 1%, approximately $10 \times$ less than the thin lens regime. While the accuracy of the semithin lens regime is a function of L_{cav}/l_{q1} , the error increases with l_{q1} , for the same value of L_{cav}/l_{q1} .

IV. CONCATENATING MULTIPLE HALF-FODO CELLS

As there is nothing special about the first half-FODO cell used to derive important constraints, the constraints extend to all half-FODO cells in a lattice, allowing for propagating equations to be formed. First, the second index describing the quadrupole length is reintroduced, describing if the quadrupole is the first or second half of the complete quadrupole unit, recall:

$$l_{q1} \rightarrow l_{q1,2}, \quad l_{q2} \rightarrow l_{q2,1}.$$

For a set of N half-FODO cells, there exists $2N$ half quadrupoles. The k strengths behave as follows:

$$\begin{aligned} k_1 &= \frac{k_2}{\left(\frac{\gamma_{r0}\beta_{r0}}{\gamma_{r1}\beta_{r1}}\right)^2} = \frac{k_3}{\left(\frac{\gamma_{r0}\beta_{r0}}{\gamma_{r1}\beta_{r1}}\right)^2} \\ &= \frac{k_4}{\left(\frac{\gamma_{r0}\beta_{r0}}{\gamma_{r1}\beta_{r1}}\right)^2 \left(\frac{\gamma_{r1}\beta_{r1}}{\gamma_{r2}\beta_{r2}}\right)^2} = \dots = \frac{k_{2N}}{\prod_{i=0}^{N-1} \left(\frac{\gamma_{ri}\beta_{ri}}{\gamma_{r(i+1)}\beta_{r(i+1)}}\right)^2}. \end{aligned} \quad (46)$$

Where we define that $k_{2N} = k_{2N+1}$ as they are two sections of the same quadrupole but separated into two half-FODO cells. From Eq. (35), the relationship between consecutive quadrupole lengths (first section) can also be determined:

$$l_{q(n),1} = \frac{\gamma_{r(n-1)}\beta_{r(n-1)}}{\gamma_{r0}\beta_{r0}} l_{q1,2}. \quad (47)$$

By defining $l_{q1,2}$ and values for the Lorentz factor, all quadrupole k strengths and first section lengths can be determined. The second section lengths of quadrupoles must now be determined.

In order to satisfy the constraint in Eq. (24), Eq. (40) is combined with the fact

$$\beta_{y1} \approx \frac{\sqrt{r}}{k_2 l_{q2,2}} \sqrt{1 + \frac{l_{q2,2}}{L_{\text{eff},2}}}, \quad (48)$$

producing a constraint on values for $L_{\text{eff},n}$:

$$L_{\text{eff},2} = \frac{\gamma_{r1}\beta_{r1}}{\gamma_{r0}\beta_{r0}} L_{\text{eff},1}. \quad (49)$$

As a constant aspect ratio was assumed, this constraint must be enforced

$$\begin{aligned} r_1 &\approx \frac{1 + L_{\text{eff},1}k_1 l_{q1,2} + k_1 l_{q1,2}^2 - \frac{L_{\text{eff},1}k_1^2 l_{q1,2}^3}{2}}{1 - L_{\text{eff},1}k_1 l_{q1,2} - k_1 l_{q1,2}^2 - \frac{L_{\text{eff},1}k_1^2 l_{q1,2}^3}{2}} \\ &\approx r_2 \approx \frac{1 + L_{\text{eff},2}k_2 l_{q2,2} + k_2 l_{q2,2}^2 - \frac{L_{\text{eff},2}k_2^2 l_{q2,2}^3}{2}}{1 - L_{\text{eff},2}k_2 l_{q2,2} - k_2 l_{q2,2}^2 - \frac{L_{\text{eff},2}k_2^2 l_{q2,2}^3}{2}}. \end{aligned} \quad (50)$$

Substituting with Eqs. (34) and (49), it is a requirement that

$$l_{q2,2} = \frac{\gamma_{r1}\beta_{r1}}{\gamma_{r0}\beta_{r0}} l_{q1,2}. \quad (51)$$

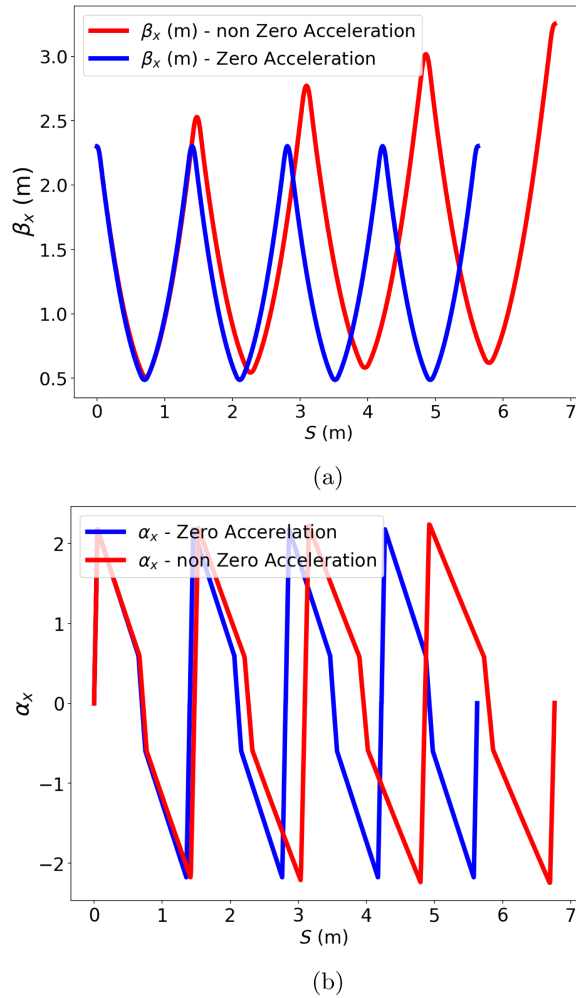
From Eq. (47), $l_{q2,1} = l_{q2,2}$. This result: quadrupole sections of the same quadrupole unit are the same length (in addition to k strength), and the maximum/minimum beam size occurs at the center point of the quadrupole unit.

In order to satisfy Eq. (49), either the drift or cavity length (or a combination of the both) can be altered within consecutive half-FODO cells [see Eq. (19)]. The required change in element length manifests differently in each element. As drift lengths are short relative to cavity lengths, the drifts become long, and the real estate gradient drops. When the constraint term is absorbed by increasing consecutive cavity lengths, the additional length does not cause a drop in real estate gradient. In fact, it can be shown that a FODO-like scheme is possible such that cavity lengths increase faster than quadrupole lengths, thus producing a lattice with higher real estate gradient than the standard FODO scheme. Figure 8 shows the change in real estate gradient for different methods to solve Eq. (49).

In this section, the FODO-like focusing scheme was explored. Given an initial set of parameters, namely the first quadrupole length, drift length, and cavity length, the value of all quadrupole lengths and k strengths is determinable, such that the limiting beam size is minimized at the cavity entrance/exit. In addition to the quadrupole parameters, consecutive cavity lengths and drift lengths are constrained such that the aspect ratio and beam size are constant at each half-FODO cell.

V. FODO RESULTS

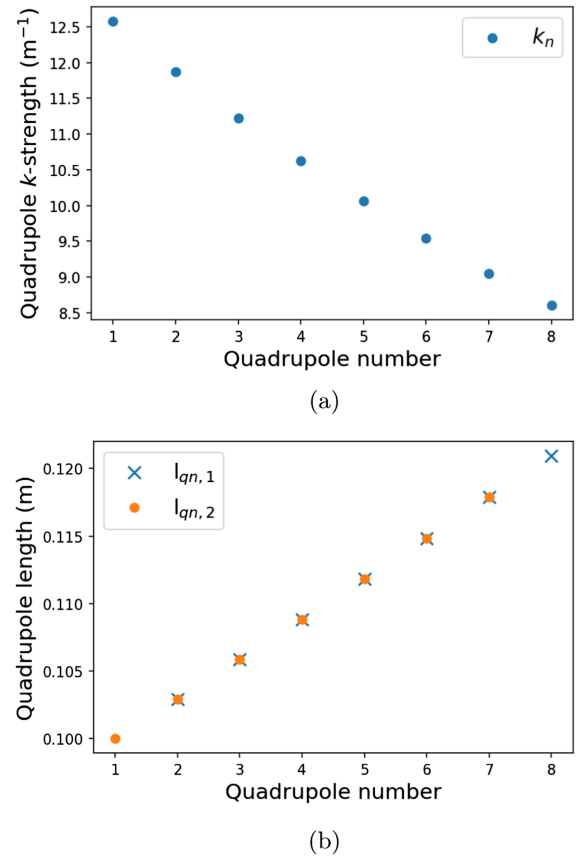
Figure 4 displays the β_x (a) and α_x (b) Twiss parameters as a function of longitudinal displacement, s , over four FODO cells. Twiss parameters are shown for both the standard (zero acceleration) and FODO-like (nonzero acceleration) lattices. The standard FODO refers to the


 FIG. 4. Twiss β (a) and α (b) functions along FODO-like lattice.

case of constant quadrupole strengths and lengths along the lattice, in addition to the drift lengths. The FODO-like lattice refers to the case where lattice parameters change as describe by Eqs. (46), (47), (49), and (51). The lattice is comprised of cavities with lengths of the order 1 m and gradients of 50 MeV/m. $l_{q1} = 0.01$ m and $l_{g1} = 0.05$ m. The maximum β_x function for a FODO-like lattice increases with s , as the Lorentz factor increases due to acceleration from rf cavities.

The total length of the FODO lattice is longer for the FODO-like lattice, as the quadrupole lengths, cavity lengths, and/or drift lengths increase with Lorentz factor, from Eqs. (33) and (49). Figure 5 demonstrates the decrease/increase in consecutive quadrupole k strength/lengths along a FODO-like lattice. The constant beam size in both transverse planes along a FODO-like lattice are shown in Fig. 6, as required.

Figure 7 displays the x phase space ellipse at the entrance of the fifth half-FODO cell as calculated by both a constant (standard FODO) and constrained (FODO-like) FODO lattices. For constant lattice parameters, the phase space


 FIG. 5. Quadrupole k strength (a) and length (b) as a function of quadrupole number in FODO-like scheme.

ellipse is over/under focused at half-FODO cell boundaries, as the constant aspect ratio and beam size constraint are not met. The constrained lattice produces a well matched ellipse at the boundary, as required. In the limit of a high number of periodic FODO cells, the standard FODO scheme remains stable, when acceleration is incorporated.

The standard FODO lattice produces larger real estate gradients to the FODO-like lattice when considering long and fixed cavity lengths. In this case, the drift length must increase along the lattice to keep Eq. (49) satisfied. As the cavity lengths are long, the correction to subsequent l_g is large, and the real estate gradient drops. In addition, increased l_g causes the beam to defocus longitudinally.

For linacs with short cavity lengths, the correction absorbed by l_g is small, and the defocusing effect is suppressed. Thus for short cavity length, the FODO-like scheme becomes an effective focusing scheme. As previously discussed, cavity lengths can be defined to increase in length, such that the FODO-like lattice has higher real estate to the standard FODO lattice. Figure 8 displays the change in cavity and drift length for three three different FODO-like lattice adopting different methods to satisfy Eq. (49). The real estate is defined as the percentage of active accelerating length relative to the total longitudinal length of the beam line. The maximum real estate is

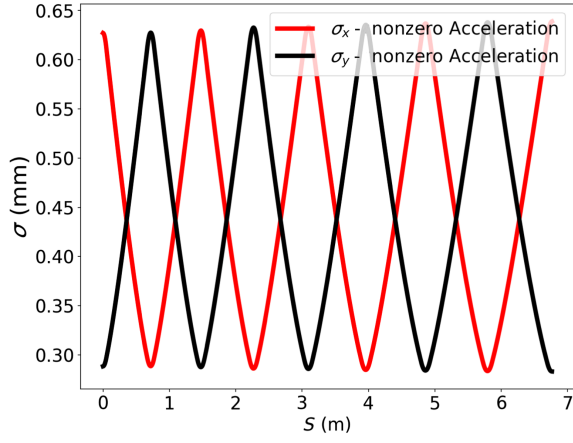


FIG. 6. Transverse beam size in the FODO-like scheme.

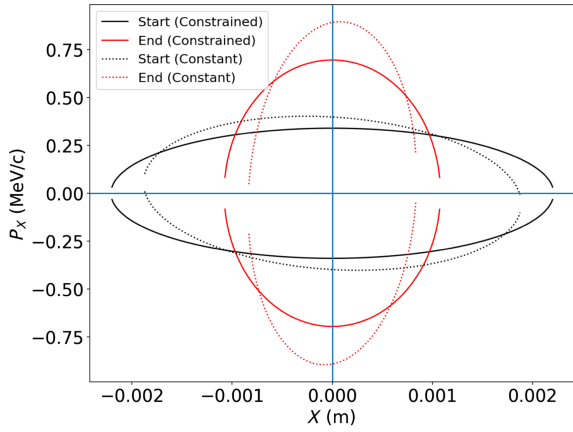


FIG. 7. Phase space ellipse at fifth half-FODO cell calculated with constant or constrained lattice parameters.

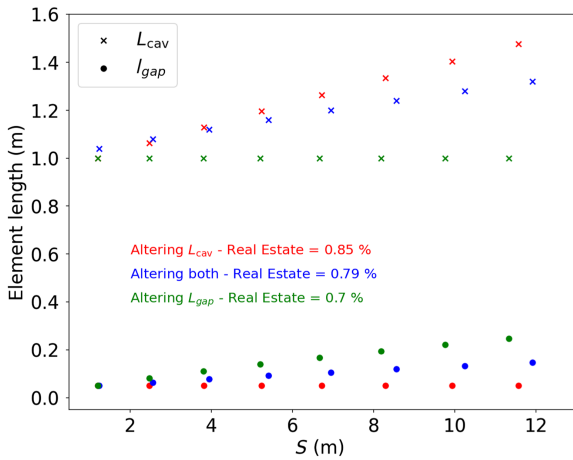


FIG. 8. Development of the cavity and drift length, for different methods of satisfying Eq. (49).

achieved by keeping l_g constant and increasing L_{cav} , as expected.

VI. MINIMUM APERTURE SCHEME

The MAS considers the focusing scheme by which a set of focusing elements are placed upstream of a cavity that orients the beam ellipse to match the acceptance ellipse of the cavity. For a given cavity length, the MAS produces the minimum cavity aperture that can be realized, for a given transverse beam emittance. A schematic of the MAS is shown Fig. 9.

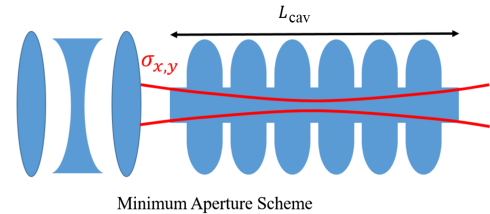
The MAS scheme realizes the case of minimum beam size at the cavity entrance/exit. The first constraint thus forces equal beam size either side of the cavity:

$$\sigma_{xc0} = \sigma_{xc1}, \quad \rightarrow \beta_{xc0} \frac{\gamma_{r1} \beta_{r1}}{\gamma_{r0} \beta_{r0}} = \beta_{xc1}. \quad (52)$$

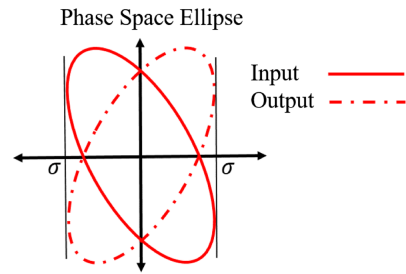
The input beta function, β_{xc0} , is a constrained value given by the beam emittance and aperture size. β_{xc1} is determinable using the Twiss parameter transform matrix [Eq. (13)]:

$$\beta_{xc1} = \frac{\gamma_{r1} \beta_{r1}}{\gamma_{r0} \beta_{r0}} (R_{11}^2 \beta_{xc0} - 2R_{11}R_{12} \alpha_{xc0} + R_{12}^2 \gamma_{xc0}). \quad (53)$$

The matrix elements R are defined by the rf cavity map shown in Eq. (12). Solving Eq. (53) for α_{xc0} produces a quadratic, solved using the quadratic formula. As there is only one set of Twiss parameters that can produce the required beam ellipse, the determinant must be zero. The results are shown below:



(a)



(b)

FIG. 9. (a) MAS schematic. (b) Input/output phase space ellipse in MAS.

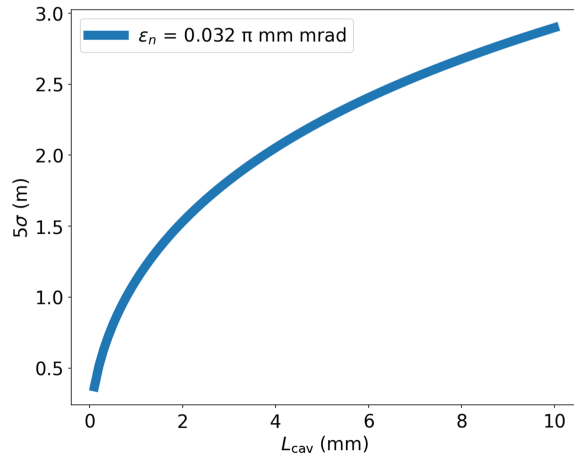


FIG. 10. Beam aperture as a function of cavity length in the MAS scheme.

$$\beta_{xc0} = L_{cav} \frac{\gamma_{r0}\beta_{r0}}{\gamma_{r1} - \gamma_{r0}} \ln \left(\frac{\gamma_{r1}\beta_{r1} + \gamma_{r1}}{\gamma_{r0}\beta_{r0} + \gamma_{r0}} \right) \approx L_{cav}, \quad (54)$$

$$\alpha_{xc0} = 1, \quad (55)$$

and

$$\gamma_{xc0} = \frac{2}{L_{cav} \frac{\gamma_{r0}\beta_{r0}}{\gamma_{r1} - \gamma_{r0}} \ln \left(\frac{\gamma_{r1}\beta_{r1} + \gamma_{r1}}{\gamma_{r0}\beta_{r0} + \gamma_{r0}} \right)}. \quad (56)$$

It can be shown that for a given transverse emittance, the minimum cavity aperture as a function of cavity length is

$$a = \sqrt{\varepsilon_n \left[\frac{L_{cav}}{\gamma_{r1} - \gamma_{r0}} \ln \left(\frac{\gamma_{r1}\beta_{r1} + \gamma_{r1}}{\gamma_{r0}\beta_{r0} + \gamma_{r0}} \right) \right]}. \quad (57)$$

Figure 10 displays the minimum cavity aperture for a 5σ beam as a function of cavity length with gradient of 50 MeV/m.

The MAS requires multiple quadrupoles to produce the required matching for the beam ellipse and thus uses more quadrupole per cavity than the FODO-like scheme. However, the MAS can produce optimal focusing schemes, where the increase in nonactive length (quadrupoles, drift lengths) is less than the increase in active cavity length.

VII. CONCLUSION

In this paper, a self-consistent framework was demonstrated that allowed the incorporation of acceleration into transverse beam dynamics studies for a proton linac machine. Two focusing schemes were developed and discussed: the FODO-like scheme and the minimum

aperture scheme. The FODO-like scheme is a simple scheme, requiring only one quadrupole per cavity. The scheme was analytically solved to minimize the beam size at the cavity entrance/exit and ensures constant beam size along the lattice. It was shown that lattice parameters must be altered along the FODO cell, to meet the design constraints for an accelerating scheme. The MAS describes the regime that matched the beam ellipse to the acceptance ellipse of a cavity, allowing for the smallest possible aperture, for a given cavity length. The MAS will require more than one quadrupole per cavity, and therefore, will only have higher real estate gradients than the FODO-like scheme in special cases.

ACKNOWLEDGMENTS

The studies presented have been funded through the Cockcroft Core Grant by STFC Grants No. ST/P002056/1 and No. ST/V001612/1.

- [1] A. Degiovanni, Future trends in linacs, CERN Yellow Reports, *Proceedings of the CAS–CERN Accelerator School on Accelerators for Medical Applications* (2017), <https://pdfs.semanticscholar.org/bca2/148907f0fba76a28962bc7a33500cb36e499.pdf>.
- [2] J. Thariat, J.-M. Hannoun-Levi, A. S. Myint, T. Vuong, and J.-P. Gérard, Past, present, and future of radiotherapy for the benefit of patients, *Nat. Rev. Clin. Oncol.* **10**, 52 (2013).
- [3] J. Llacer, A. Chatterjee, E. L. Alpen, W. Saunders, S. Andraea, and H. C. Jackson, Imaging by injection of accelerated radioactive particle beams., *IEEE Trans. Med. Imaging* **3**, 80 (1984).
- [4] C. Bert, N. Saito, A. Schmidt, N. Chaudhri, D. Schardt, and E. Rietzel, Target motion tracking with a scanned particle beam, *Med. Phys.* **34**, 4768 (2007).
- [5] U. Schneider and E. Pedroni, Proton radiography as a tool for quality control in proton therapy, *Med. Phys.* **22**, 353 (1995).
- [6] J. O. Archambeau, G. W. Bennett, and G. S. Levine, Application of proton radiation therapy, *IEEE Trans. Nucl. Sci.* **20**, 1007 (1973).
- [7] A. Wolski, *Beam Dynamics in High Energy Particle Accelerators* (World Scientific, Singapore, 2014).
- [8] M. Southerby and R. Apsimon, Fast tracking of 6D particle phase space using the FC2CT algorithm for rf cavities, *Phys. Rev. Accel. Beams* (to be published).
- [9] J. Rosenzweig and L. Serafini, Transverse particle motion in radio-frequency linear accelerators, *Phys. Rev. E* **49**, 1599 (1994).
- [10] R. W. D. Nickalls, Viete, descartes and the cubic equation, *Mathemat. Gazette* **90**, 203 (2006).